Acta Crystallographica Section D
Biological Crystallography
ISSN 0907-4449

Crystallization of the actin-binding domain of human α-actinin: analysis of microcrystals of SeMet-labelled protein

Fredrik Ekström,[a] Gunter Stier[b] and Uwe H. Sauer[a]*

[a]Umeå Center for Molecular Pathogenisis, UCMP, Umeå Universit, SE-901 87 Umeå, Sweden, and [b]EMBL, Meyerhofstrasse 1, D-69017 Heidelberg, Germany

Correspondence e-mail: uwe@ucmp.umu.se

Received 16 October 2002
Accepted 22 January 2003

α-Actinin forms antiparallel homodimers that cross-link actin filaments from adjacent sarcomeres within the Z-discs of striated muscle. The N-terminal actin-binding domain (ABD) is composed of two calponin homology (CH) domains followed by four spectrin-like repeats and a calmodulin-like EF-hand domain at the C-terminus. The ABD of human α-actinin crystallizes in space group $P2_1$, with unit-cell parameters a = 101.9, b = 38.4, c = 154.9 Å, β = 109.2°. A complete native data set from a native crystal was collected extending to 2.0 Å resolution and a single-wavelength anomalous dispersion (SAD) data set to 2.9 Å resolution was collected from a selenomethionine-labelled microcrystal using the microfocusing beamline ID-13 at the ESRF. Analysis of the anomalous contribution shows a rapid decrease in the $\sigma_{\rm normal}/\sigma_{\rm anomal}$ ratio owing to radiation damage.

1. Introduction

Skeletal muscle α-actinin plays an important role during muscle assembly (Young & Gautel, 2000) and is one of the major organizers within the muscle Z-disc, where it cross-links actin filaments and the giant filamentous protein titin (Ohtsuka *et al.*, 1997; Tang *et al.*, 2001). The α-actinin protein dimerizes *via* the four central spectrin-like repeats (Sr-repeats) (Djinovic Carugo *et al.*, 1999; Ylanne *et al.*, 2001) to form a rod-like antiparallel homodimer. Actin binding is accomplished through a tandem arrangement of two calponin homology domains (CH1 and CH2) located in the N-terminal actin-binding domain (ABD), whereas the two EF-hand motives at the C-terminus interact with titin (Banuelos *et al.*, 1998; Joseph *et al.*, 2001). The relative orientation of the tandem CH domains can vary owing to a flexible linker helix. In the case of human fimbrin (Goldsmith *et al.*, 1997) the CH1 and CH2 domains adopt compact packing, whereas the two CH domains of dystrophin (Norwood *et al.*, 2000) and utrophin (Keep *et al.*, 1999) adopt a more open conformation. Detailed information about the structure and relative conformation of the CH1 and CH2 domains will provide a deeper understanding of the mechanism of interaction with actin filaments within the muscle Z-disc.

A standard way to determine protein structures is by using crystals of selenomethionine (SeMet) labelled protein in a multiple-wavelength anomalous dispersion (MAD) or single-wavelength anomalous dispersion (SAD) experiment. However, the crystallization of SeMet-labelled protein can prove difficult. In the case of the α-actinin ABD, the SeMet-labelled protein yielded crystals that were unsuitable for traditional data collection. However, recent advances in instrumentation made it possible to collect data from such microcrystals (Cusack *et al.*, 1998; Perrakis *et al.*, 1999). In this study, we present the crystallization and preliminary diffraction data analysis of native and SeMet-labelled α-actinin ABD.

2. Materials and methods

2.1. Cloning, expression and purification

The DNA segment coding for residues 1–267 of the actin-binding domain of human skeletal muscle α-actinin-2 isoform, ACTN, (DDBJ/EMBL/GenBank accession No. M86406) was amplified from a human skeletal muscle cDNA library by PCR using the 5′ primer TTT CCA TGG GCC AGA TAG AGC CCG GCG TGCA and the 3′ primer TTT GGT ACC TTA CTC CGC GCC CGC AAA AGC GT. The second amino acid of the native peptide sequence was changed from an Asp to a Gly residue (N2G) in order to introduce an internal *Nco*I site. The PCR product was cloned into the *Nco*I and *Kpn*I sites of a modified pET24d expression vector that contained coding sequences for an N-terminal His_6 tag followed by glutathione-*S*-transferase (GST) and a recognition site for tobacco etch virus (TEV) protease preceding the *Nco*I site. Subsequent DNA sequencing detected a single-base mutation changing Glu37 to Lys in the expressed protein (ABD-E37K). The wild-type gene (ABD-wt) was recloned and the correct

sequence was confirmed. Subsequent experiments were carried out with both clones in parallel under identical conditions. Plasmids were transformed into *Escherichia coli* strain BL21 (DE3) (Novagen Inc.) for protein production. The cells were cultured at 310 K in Luria–Bertani (LB) broth supplemented with 30 µg ml^{-1} kanamycin to a density of A_{600} = 0.8–1.0 OD, at which point the temperature was reduced to 293 K and protein expression was induced overnight with 0.2 m*M* isopropyl thiogalactopyranoside (IPTG). The culture was pelleted and stored at 193 K. For purification, freshly thawed cells were resuspended in lysis buffer containing 20 m*M* Tris pH 8.0, 200 m*M* NaCl. Cells were lysed by sonication in the presence of lysozyme and DNaseI. The cell lysate was centrifuged at 30 000*g* for 50 min. The supernatant was incubated with Ni–NTA–agarose (Qiagen) for 15 min and applied to an Econo chromatography column (BioRad). After equilibrating the column with 20 m*M* Tris pH 8.0, 200 m*M* NaCl, unspecifically bound protein was removed by increasing the salt concentration to 1.0 *M* NaCl. The His-tagged protein was step-eluted from the Ni–NTA matrix in 20 m*M* Tris pH 8.0, 200 m*M* NaCl, 500 m*M* imidazole. By addition of His_6-tagged TEV protease during the dialysis step against low imidazole buffer (20 m*M* Tris pH 8.0, 50 m*M* NaCl), the His_6-GST tag was removed from the ABD fusion protein. The cleaved ABD eluted with the flowthrough of a second Ni–NTA column. Further purification using a MonoQ 10/10 column (Amersham Pharmacia Biotech) resulted in pure protein. In the last step, the ABD was concentrated by centrifugation using Centriprep-10 concentrators (Amicon). The SeMet-labelled ABD was produced in a methionine-auxotropic strain of *E. coli*, B834 (DE3) (Novagen),

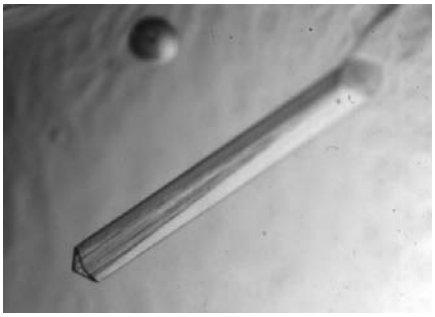

Figure 1
The rod-like ABD-E37K crystals grew to overall dimensions of 0.06 × 0.06 × 0.7 mm overnight at 291 K. The crystals belong to space group $P2_1$, with unit-cell parameters a = 101.9, b = 38.4, c = 154.9 Å, β = 109.2°. The morphology of the selenomethionine-labelled protein crystals is similar, but they have considerably smaller dimensions.

Table 1
Data-collection and processing statistics.

Values for the highest resolution shell are given in parentheses.

	Native	SeMet†
Beamline used	I711, MAX-lab	ID13, ESRF
Space group	$P2_1$	$P2_1$
Unit-cell parameters (Å, °)	a = 101.90, b = 38.40, c = 154.90, β = 109.20	a = 102.5, b = 39.1, c = 158.3, β = 108.9
Wavelength (Å)	1.0854	0.9715
Resolution range (Å)	45–2.0 (2.15–2.0)	50–2.9 (3.0–2.9)
Total reflections	502772 (71170)	96654 (14130)
Unique reflections	72560 (8620)	49086 (6101)
$I/\sigma(I)$	14.3 (7.1)	5.5 (2.6)
Completeness (%)	96.8 (93.6)	87.6 (73.3)
R_{merge}‡ (%)	8.1 (31.8)	10.3 (35.6)

† Data range 1–180°. ‡ R_{merge} $(I) = [\sum_{\mathbf{h}} \sum_{i=1}^{N} |I_i(\mathbf{h}) - \langle(\mathbf{h})\rangle|/ \sum_{\mathbf{h}} \sum_{i=1}^{N} I_i(\mathbf{h})| \times 100$.

following a standard protocol (Hendrickson *et al.*, 1990). Purification was identical to that of the unlabelled protein. Complete incorporation of nine SeMet residues was verified by mass spectrometry [$MW_{(ABD\text{-}E37K)}$ = 30 924 Da, $MW_{(Se\text{-}ABD\text{-}E37K)}$ = 31 345 Da, ΔMW = 421 Da and $\Delta MW_{Se/S}$ = 46.9 Da].

2.2. Crystallization and data collection

Crystallization screens of ABD-wt and ABD-E37K were initially performed with commercially available solutions (Crystal Screen I and II, Hampton Research) using the hanging-drop vapour-diffusion method. Crystallization setups contained 2 µl of a 10 mg ml^{-1} ABD solution and 2 µl mother liquor mixed on a cover slip and sealed over a reservoir containing 500 µl mother liquor. The wild-type protein underwent further screening exploring different protein concentration ranges (6–20 mg ml^{-1}) and different crystallization temperatures (277, 285, 291 and 297 K). Initially, thin needle-shaped ABD-E37K crystals appeared overnight from 30% PEG 5000 MME, 0.1 *M* MES pH 6.5, 0.2 *M* ammonium sulfate (condition No. 26 of Crystal Screen II) at 291 K. These conditions were further refined in order to optimize the size and diffraction quality of the ABD-E37K crystals.

The crystals were mounted free-standing in a nylon loop (Sauer & Ceska, 1997) and flash-cooled to 100 K in a cold nitrogen-gas stream using an Oxford Cryosystems cryo head. Native data were collected from cryocooled ABD-E37K crystals using a MAR345 image-plate detector (X-ray Research GmbH) at beamline I711, MAX-lab, Sweden. In addition, a SAD data set from a selenomethionine-labelled microcrystal was collected at microfocusing beamline ID-13 (beam size 15 × 15 µm) at the European Synchrotron Radiation Facility (ESRF), France. Data collection was performed at a wavelength of λ = 0.9715 Å (E = 12.7620 keV), a value slightly above the Se K edge (λ = 0.9795 Å; E = 12.6578 keV). This wavelength was chosen to make sure that an anomalous contribution was recorded, since the wavelength at ID-13 had to be adjusted by changing the gap distance of the undulator magnets. The data set was collected as a continuous series of 1° oscillation images covering a rotation range of 180° recorded using a 130 mm diameter MAR CCD detector (X-ray Research GmbH). All intensities were indexed, integrated and scaled with *XDS*/*XSCALE* (Kabsch, 1988).

3. Results and discussion

The purification of the ABD of human α-actinin (ABD-wt and ABD-E37K) yielded about 20 mg of pure protein per litre of bacterial cell culture. The protein elutes as a monomer from a size-exclusion column and shows a monodisperse distribution when analysed by dynamic light scattering (Protein Solutions, data not shown). No differences in affinity for F-actin were detectable between ABD-wt and ABD-E37K as confirmed by pull-down experiments (data not shown). Surprisingly, only the ABD-E37K protein yielded crystals suitable for X-ray diffraction studies, while none of the conditions tested for ABD-wt resulted in crystalline material. Initially, ABD-E37K crystallized in the form of thin needles overnight from 30% PEG 5000 MME, 0.1 *M* MES pH 6.5, 0.2 *M* ammonium sulfate (condition No. 26 of Crystal Screen II) at 291 K. Exploring the initial ABD-E37K crystallization conditions further showed that crystals grew in the pH range 5–9 and from PEG concentrations between 24 and 30%. The mother liquor of the optimized growth condition contains 26% PEG 5000 MME, 0.1 *M* MES pH 6.3, 0.2 *M* ammonium sulfate. ABD-E37K crystals

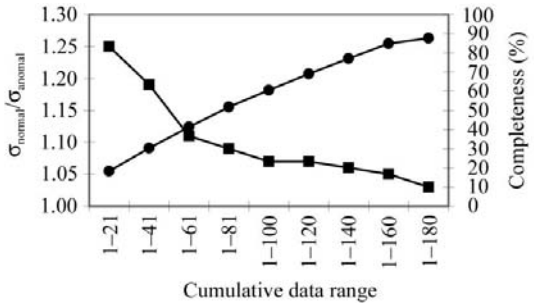

Figure 2
Decay of the anomalous signal during data collection. Depicted along the *y* axis are the ratio $\sigma_{normal}/\sigma_{anomal}$ (squares) and the completeness of the data (circles). The corresponding data-processing intervals are shown on the *x* axis. σ_{normal} is the mean value of $\sigma(I)$ for acentric reflections assuming Friedel's law to be true and σ_{anomal} is the mean value for $\sigma(I)$ for acentric reflections assuming Friedel's law to be false. Values of $\sigma_{normal}/\sigma_{anomal} > 1$ indicates an anomalous scattering contribution to the intensities. Values are taken from processing with *XDS* (Kabsch, 1988).

grew overnight at 293 K and reached final dimensions of 0.06 × 0.06 × 0.7 mm. They display a characteristic morphology with a central groove or hole extending along the central axis of the crystal (Fig. 1) and diffract to a resolution of 2.0 Å (Table 1).

Crystals of ABD-E37K labelled with selenomethionine grew under similar conditions as the native crystals. They showed a rod-like morphology with considerable smaller dimensions (15 × 15 × 100 µm). Neither seeding nor the addition of reducing agents such as 2-mercapthoethanol or DL-dithiothreitol affected their size. Because of their small dimensions, we attempted SAD data collection at the microfocusing beamline ID13, ESRF (Cusack *et al.*, 1998; Perrakis *et al.*, 1999). The microcrystals diffracted to 2.9 Å resolution and yielded good data-processing statistics (Table 1). Compared with the unit-cell parameters of the native crystals, the SeMet protein crystals showed increases in the lengths of the *a*, *b* and *c* axes of about 0.6, 1.8 and 2.2%, respectively. This could be because of the nine SeMet residues incorporated into the protein. Although the diffraction data was of good quality, it only contained a weak anomalous signal, with an overall $\sigma_{normal}/\sigma_{anomal}$ ratio of about 1.05. Monitoring the ratio as data-collection progressed showed a rapid decrease in the signal, which can be attributed to radiation damage (Fig. 2). A simple way to reduce the effect of radiation damage in the case of a rod-like crystal would be to frequently translate the crystal in the beam in order to irradiate an undamaged volume or to use several crystals for data collection. The frequency of translation of the crystal will depend on the X-ray photon flux passing through the irradiated volume. To further improve the SAD data quality, we suggest the use of the reverse-beam geometry for each crystal position in order to collect Friedel pairs. In the case of the SeMet-labelled ABD-E37K crystals it would have been appropriate to translate the crystal after about 20° of data collection (see Fig. 2), *e.g.* after collecting data from φ to φ + 10° followed by φ + 180 to φ + 190°.

The authors would like to thank Drs Anastassis Perrakis and Stephen Cusack from the EMBL Grenoble Outstation as well as Dr Christian Riekel and the staff of ESRF beamline ID13 for expert help with microfocusing data collection. The travel expenses for the microfocus TC-89 project were covered by an EMBL TMR grant. The authors also acknowledge Yngve Cerenius and the staff of beamline I711, MAX-lab, Lund University, Sweden. This work was supported by a grant from the J. C. Kempe foundation.

References

Banuelos, S., Saraste, M. & Djinovic Carugo, K. (1998). *Structure*, **6**, 1419–1431.
Cusack, S., Belrhali, H., Bram, A., Burghammer, M., Perrakis, A. & Riekel, C. (1998). *Nature Struct. Biol.* **5**, 634–637.
Djinovic Carugo, K., Young, P., Gautel, M. & Saraste, M. (1999). *Cell*, **98**, 537–546.
Goldsmith, S. C., Pokala, N., Shen, W., Fedorov, A. A., Matsudaira, P. & Almo, S. C. (1997). *Nature Struct. Biol.* **4**, 708–712.
Hendrickson, W. A., Horton, J. R. & LeMaster, D. M. (1990). *EMBO J.* **9**, 1665–1672.
Joseph, C., Stier, G., O'Brien, R., Politou, A. S., Atkinson, R. A., Bianco, A., Ladbury, J. E., Martin, S. R. & Pastore, A. (2001). *Biochemistry*, **40**, 4957–4965.
Kabsch, W. (1988). *J. Appl. Cryst.* **21**, 916–924.
Keep, N. H., Winder, S. J., Moores, C. A., Walke, S., Norwood, F. L. & Kendrick-Jones, J. (1999). *Structure Fold Des.* **7**, 1539–1546.
Norwood, F. L., Sutherland-Smith, A. J., Keep, N. H. & Kendrick-Jones, J. (2000). *Structure Fold Des.* **8**, 481–491.
Ohtsuka, H., Yajima, H., Maruyama, K. & Kimura, S. (1997). *FEBS Lett.* **401**, 65–67.
Perrakis, A., Cipriani, F., Castagna, J. C., Claustre, L., Burghammer, M., Riekel, C. & Cusack, S. (1999). *Acta Cryst.* D**55**, 1765–1770.
Sauer, U. H. & Ceska, T. A. (1997). *J. Appl. Cryst.* **30**, 71–72.
Tang, J., Taylor, D. W. & Taylor, K. A. (2001). *J. Mol. Biol.* **310**, 845–858.
Ylanne, J., Scheffzek, K., Young, P. & Saraste, M. (2001). *Structure*, **9**, 597–604.
Young, P. & Gautel, M. (2000). *EMBO J.* **19**, 6331–6340.